Well-Balanced Central-Upwind Schemes for the Euler Equations with Gravitation

Alina Chertock*, Shumo Cui†, Alexander Kurganov‡,
Şeyma Nur Özcan§ and Eitan Tadmor¶

Abstract

In this paper, we develop a second-order well-balanced central-upwind scheme for the Euler equations of gas dynamics with gravitation. The proposed scheme is capable of exactly preserving steady-state solutions expressed in terms of a nonlocal equilibrium variable. A crucial step in the construction of the second-order scheme is a well-balanced piecewise linear reconstruction of equilibrium variables, which is combined with a well-balanced evolution in time, achieved by reducing the amount of numerical viscosity (present at the central-upwind scheme) in the areas where the flow is at (near) steady-state regime. We show the performance of our newly developed central-upwind scheme and demonstrate importance of perfect balance between the fluxes and gravitational forces on a number of one- and two-dimensional examples.

Key words: Euler equations of gas dynamics with gravitation, well-balanced scheme, equilibrium variables, central-upwind scheme, piecewise linear reconstruction.
AMS subject classification: 76M12, 65M08, 35L65, 76N15, 86A05.

1 Introduction

We consider the Euler equations of gas dynamics with gravitation, which can be written in the two-dimensional (2-D) case as

$$\boldsymbol{q}_t + \boldsymbol{F}(\boldsymbol{q})_x + \boldsymbol{G}(\boldsymbol{q})_y = \boldsymbol{S}(\boldsymbol{q}), \tag{1.1}$$

*Department of Mathematics, North Carolina State University, Raleigh, NC, 27695, USA; chertock@math.ncsu.edu
†Mathematics Department, Tulane University, New Orleans, LA 70118, USA; scui2@tulane.edu
‡Mathematics Department, Tulane University, New Orleans, LA 70118, USA; kurganov@math.tulane.edu
§Department of Mathematics, North Carolina State University, Raleigh, NC, 27695, USA; snozcan@ncsu.edu
¶Department of Mathematics, Center of Scientific Computation and Mathematical Modeling (CSCAMM), Institute for Physical sciences and Technology (IPST), University of Maryland, College Park, MD, 20742, USA; tadmor@cscamm.umd.edu

where

$$\boldsymbol{q} := \begin{pmatrix} \rho \\ \rho u \\ \rho v \\ E \end{pmatrix} \tag{1.2}$$

is a vector of conservative variables, and

$$\boldsymbol{F}(\boldsymbol{q}) = \begin{pmatrix} \rho u \\ \rho u^2 + p \\ \rho uv \\ u(E+p) \end{pmatrix} \quad \text{and} \quad \boldsymbol{G}(\boldsymbol{q}) := \begin{pmatrix} \rho v \\ \rho uv \\ \rho v^2 + p \\ v(E+p) \end{pmatrix} \tag{1.3}$$

are the fluxes in the x- and y-directions, and

$$\boldsymbol{S}(\boldsymbol{q}) = \begin{pmatrix} 0 \\ -\rho\phi_x \\ -\rho\phi_y \\ -\rho u\phi_x - \rho v\phi_y \end{pmatrix} \tag{1.4}$$

is the source term. Here, ρ is the density, u and v are the x- and y-velocities, E is the total energy, p is the pressure and ϕ is the time-independent linear gravitational potential.

The system (1.1)–(1.4) is closed using the following equation of state (EOS):

$$E = \frac{p}{\gamma - 1} + \frac{\rho}{2}(u^2 + v^2), \tag{1.5}$$

where γ stands for the specific heat ratio. Here, we consider a physically relevant case, in which the gravitational potential is taken in the y-direction only, that is, $\phi_x = 0$ and $\phi_y = g$.

The system of balance laws (1.1)–(1.5) is used to model astrophysical and atmospheric phenomena in many fields including supernova explosions [16], (solar) climate modeling and weather forecasting [3]. In many physical applications, solutions of the system (1.1)–(1.5) are small perturbations of the steady states. Capturing such solutions numerically is a challenging task since the size of these perturbations may be smaller than the size of the truncation error on a coarse grid. To overcome this difficulty, one can use very fine grid, but in many physically relevant situations, this may be unaffordable. Therefore, it is important to design a well-balanced numerical method, that is, the method which is capable of exactly preserving some steady state solutions. Then, perturbations of these solutions will be resolved on a coarse grid in a non-oscillatory way.

Well-balanced schemes were introduced in [14] and mainly developed in the context of shallow water equations, for details, see, e.g., [1, 2, 4, 6, 8–11, 15, 17, 20, 23, 28–31, 37]. Some of these schemes have been extended for the Euler equations with gravitational fields. In [24], quasi-steady wave-propagation methods were developed for models with a static gravitational field. In [3], well-balanced finite-volume methods, which preserve a certain class of steady states, were derived for nearly hydrostatic flows. In [26,34,38], gas-kinetic schemes were extended to the

multidimensional gas dynamic equations and well-balanced numerical methods were developed for problems, in which the gravitational potential was modeled by a piecewise step function. More recently, higher order finite-difference methods for the gas dynamics with gravitation were introduced in [36].

Our goal is to develop a well-balanced numerical method capable of exactly preserving the steady state solutions, which can be derived as follows. Consider, for simplicity, a one-dimensional (1-D) version of the system (1.1)–(1.5):

$$\boldsymbol{q}_t + \boldsymbol{G}(\boldsymbol{q})_y = \boldsymbol{S}(\boldsymbol{q}), \tag{1.6}$$

where

$$\boldsymbol{q} := \begin{pmatrix} \rho \\ \rho v \\ E \end{pmatrix}, \quad \boldsymbol{G}(\boldsymbol{q}) := \begin{pmatrix} \rho v \\ \rho v^2 + p \\ v(E+p) \end{pmatrix}, \quad \boldsymbol{S}(\boldsymbol{q}) := \begin{pmatrix} 0 \\ -\rho g \\ -\rho v g \end{pmatrix}, \quad E = \frac{p}{\gamma - 1} + \frac{\rho v^2}{2}. \tag{1.7}$$

The steady-state solutions of (1.6), (1.7) can be obtained by solving the time-independent system $\boldsymbol{G}(\boldsymbol{q})_y = \boldsymbol{S}(\boldsymbol{q})$. To this end, we first incorporate the source term $-\rho g$ into the flux, introduce a new global variable w,

$$w := p + R, \quad R(y,t) := g \int\limits_y^{\infty} \rho(\xi, t)\, d\xi, \tag{1.8}$$

and rewrite the system $\boldsymbol{G}(\boldsymbol{q})_y = \boldsymbol{S}(\boldsymbol{q})$ as

$$\begin{cases} (\rho v)_y = 0, \\ (\rho v^2 + w)_y = 0, \\ (v(E+p))_y = -\rho v g. \end{cases} \tag{1.9}$$

It then immediately follows that the simplest steady state of (1.9), (1.8) is the motionless one, for which

$$v \equiv 0 \quad \text{and} \quad w \equiv \text{Const}. \tag{1.10}$$

The corresponding 2-D steady state is

$$u = v \equiv 0 \quad \text{and} \quad w \equiv \text{Const}. \tag{1.11}$$

In this paper, we develop a new well-balanced central-upwind (CU) scheme for the Euler equations with gravitation. CU schemes were initially introduced in [21] for hyperbolic systems of conservation laws, further developed in [18, 19, 22] and extended to systems of balance laws in [2, 4–7, 17, 20]. The CU schemes are Godunov-type finite-volume methods that are efficient, highly accurate and do not require any (approximate) Riemann problem solver (the latter makes the CU schemes applicable in a "black-box manner" to a wide variety of multidimensional hyperbolic systems of conservation and balance laws). In the CU schemes, the numerical solution is realized in terms of cell averages of the conservative variables ($\boldsymbol{q} := (\rho, \rho v, E)^T$ or $\boldsymbol{q} := (\rho, \rho u, \rho v, E)^T$ for the 1-D and 2-D Euler equations, respectively). The cell averages are used to construct a global piecewise polynomial approximation of the numerical solution,

which is then used to evolve the computed solution in time. Unfortunately, the CU schemes implemented using a reconstruction procedure of the conservative variables do not posses the well-balanced property. We therefore modify the reconstruction step and introduce a special reconstruction based on the equilibrium variables, $(\rho, \rho v, w)^T$ (or $(\rho, \rho u, \rho v, w)^T$ in 2-D) rather than the conservative ones. This results in a well-balanced CU scheme for the Euler equations with gravitation.

The paper is organized as follows. In §2 and §3, we develop the well-balanced CU schemes for 1-D and 2-D Euler equations with gravitation. Special 1-D and 2-D well-balanced reconstructions are presented in §2.2.1 and 3.1.1, respectively. In §4, we present a number of 1-D and 2-D numerical examples.

2 One-Dimensional Numerical Method

In this section, we first (§2.1) briefly describe the semi-discrete CU scheme from [19] and then (§2.2) derive its well-balanced modification for the 1-D Euler equations with gravitation.

2.1 Second-Order Semi-Discrete Central-Upwind Scheme

For simplicity, we partition the computational domain into finite-volume cells $C_k := [y_{k-\frac{1}{2}}, y_{k+\frac{1}{2}}]$ of size $|C_k| = \Delta y$ centered at $y_k = k\Delta y$, $k = k_L, \ldots, k_R$, and the cell interfaces are denoted by $y_{k\pm\frac{1}{2}} := (k \pm 1/2)\Delta y$. We assume that at time level t, the cell averages of the numerical solution, $\overline{\boldsymbol{q}}_k(t) := \frac{1}{\Delta y}\int_{C_k} \boldsymbol{q}(y,t)\,dy$, are available.

A semi-discrete CU scheme from [19] applied to (1.6), (1.7) is the following system of ODEs:

$$\frac{d}{dt}\overline{\boldsymbol{q}}_k = -\frac{\boldsymbol{\mathcal{G}}_{k+\frac{1}{2}} - \boldsymbol{\mathcal{G}}_{k-\frac{1}{2}}}{\Delta y} + \overline{\boldsymbol{S}}_k, \tag{2.1}$$

where

$$\boldsymbol{\mathcal{G}}_{k+\frac{1}{2}} := \frac{b^+_{k+\frac{1}{2}}\boldsymbol{G}(\boldsymbol{q}^{\rm N}_k) - b^-_{k+\frac{1}{2}}\boldsymbol{G}(\boldsymbol{q}^{\rm S}_{k+1})}{b^+_{k+\frac{1}{2}} - b^-_{k+\frac{1}{2}}} + \beta_{k+\frac{1}{2}}\left(\boldsymbol{q}^{\rm S}_{k+1} - \boldsymbol{q}^{\rm N}_k\right), \quad \beta_{k+\frac{1}{2}} := \frac{b^+_{k+\frac{1}{2}}b^-_{k+\frac{1}{2}}}{b^+_{k+\frac{1}{2}} - b^-_{k+\frac{1}{2}}}, \tag{2.2}$$

are numerical fluxes, and

$$\overline{\boldsymbol{S}}_k = (0, -g\overline{\rho}_k, -g(\overline{\rho v})_k)^T$$

are approximations of the cell averages of the source term.

In (2.2), $\boldsymbol{q}^{\rm N}_k$ and $\boldsymbol{q}^{\rm S}_{k+1}$ are the one-sided point values of the computed solution at cell interfaces $y = y_{k+\frac{1}{2}}$. To construct a second-order scheme, these variables are to be calculated using the piecewise linear reconstruction

$$\widetilde{\boldsymbol{q}}(y) = \sum_k \left(\overline{\boldsymbol{q}}_k + (\boldsymbol{q}_y)_k(y - y_k)\right)\cdot\chi_{C_k}(y), \tag{2.3}$$

where χ_{C_k} is a characteristic function of the interval C_k. We then obtain

$$\boldsymbol{q}^{\rm N}_k := \widetilde{\boldsymbol{q}}(y_{k+\frac{1}{2}} - 0) = \overline{\boldsymbol{q}}_k + \frac{\Delta y}{2}(\boldsymbol{q}_y)_k, \quad \boldsymbol{q}^{\rm S}_{k+1} := \widetilde{\boldsymbol{q}}(y_{k+\frac{1}{2}} + 0) = \overline{\boldsymbol{q}}_{k+1} - \frac{\Delta y}{2}(\boldsymbol{q}_y)_{k+1}. \tag{2.4}$$

To avoid oscillations, the vertical slopes in (2.4), $(\boldsymbol{q}_y)$, are to be computed using a nonlinear limiter applied to the cell averages $\{\overline{\boldsymbol{q}}_k\}$. In all of the numerical experiments presented in §4, we have used a generalized minmod limiter (see, e.g., [25,27,33,35]) applied in the component-wise manner:

$$(\boldsymbol{q}_y)_k = \text{minmod}\left(\theta\,\frac{\overline{\boldsymbol{q}}_{k+1}-\overline{\boldsymbol{q}}_k}{\Delta y},\ \frac{\overline{\boldsymbol{q}}_{k+1}-\overline{\boldsymbol{q}}_{k-1}}{2\Delta y},\ \theta\,\frac{\overline{\boldsymbol{q}}_k-\overline{\boldsymbol{q}}_{k-1}}{\Delta y}\right), \tag{2.5}$$

where the minmod function is defined by

$$\text{minmod}(z_1,z_2,\ldots) := \begin{cases} \min(z_1,z_2,\ldots), & \text{if } \ z_i>0 \ \ \forall i,\\ \max(z_1,z_2,\ldots), & \text{if } \ z_i<0 \ \ \forall i,\\ 0, & \text{otherwise,}\end{cases} \tag{2.6}$$

and the parameter $\theta\in[1,2]$ controls the amount of numerical dissipation: The use of larger values of θ typically leads to less dissipative, but more oscillatory scheme.

Finally, the one-sided local speeds of propagation, $b^{\pm}_{k+\frac12}$, are estimated using the smallest and largest eigenvalues of the Jacobian $\frac{\partial \boldsymbol{G}}{\partial \boldsymbol{q}}$:

$$b^+_{k+\frac12} = \max\left(v^{\rm N}_k+c^{\rm N}_k,\ v^{\rm S}_{k+1}+c^{\rm S}_{k+1},\ 0\right),\quad b^-_{k+\frac12} = \min\left(v^{\rm N}_k-c^{\rm N}_k,\ v^{\rm S}_{k+1}-c^{\rm S}_{k+1},\ 0\right), \tag{2.7}$$

where the velocities, $v^{\rm N}_k$ and $v^{\rm S}_{k+1}$, are obtained using the identity $v\equiv(\rho v)/\rho$, $c^{\rm N}_k$ and $c^{\rm S}_{k+1}$ are the speeds of sound defined by $c^2=\gamma p/\rho$, and the pressures, $p^{\rm N}_k$ and $p^{\rm S}_{k+1}$, are obtained using the EOS (1.7).

Unfortunately, the CU scheme (2.1)–(2.7) is not capable of exactly preserving the steady-state solution (1.10). Indeed, substituting (1.10) into (2.1)–(2.2) and noting that $b^+_{k+\frac12}=-b^-_{k+\frac12}$, $\forall k$, we obtain the ODE system

$$\begin{cases} \dfrac{d\overline{\rho}_k}{dt} = -\dfrac{\beta_{k+\frac12}(\rho^{\rm S}_{k+1}-\rho^{\rm N}_k)-\beta_{k-\frac12}(\rho^{\rm S}_k-\rho^{\rm N}_{k-1})}{\Delta y},\\[2ex] \dfrac{d(\overline{\rho v})_k}{dt} = -\dfrac{(p^{\rm S}_{k+1}+p^{\rm N}_k)-(p^{\rm S}_k+p^{\rm N}_{k-1})}{2\Delta y},\\[2ex] \dfrac{d\overline{E}_k}{dt} = -\dfrac{\beta_{k+\frac12}(p^{\rm S}_{k+1}-p^{\rm N}_k)-\beta_{k-\frac12}(p^{\rm S}_k-p^{\rm N}_{k-1})}{(\gamma-1)\Delta y},\end{cases} \tag{2.8}$$

whose RHS does not necessarily vanish and hence the steady state would not be preserved at the discrete level. We would like to stress that even for the first-order version of the CU scheme (2.1)–(2.7), that is, when $(q_y)_k\equiv 0$ in (2.3), (2.4), the RHS of (2.8) does not vanish. This means that the lack of balance between the numerical flux and source terms is a fundamental problem of the scheme. We also note that for smooth solutions, the balance error in (2.8) is expected to be of order $(\Delta y)^2$, but a coarse grid solution may contain large spurious waves.

2.2 Well-Balanced Central-Upwind Scheme

In this section, we present a well-balanced modification of the CU scheme from §2.1. The new scheme will be developed by first introducing well-balanced reconstruction performed on the

equilibrium variables rather than the conservative ones and then deriving modified formulae for the numerical fluxes and sources.

To this end, we once again incorporate the source term $-\rho g$ into the flux and rewrite the system (1.6)–(1.7) as follows:

$$\begin{cases} \rho_t + (\rho v)_y = 0, \\ (\rho v)_t + (\rho v^2 + w)_y = 0, \\ E_t + (v(E+p))_y = -\rho v g, \end{cases} \tag{2.9}$$

which can be put into the vector form (1.6) with

$$\boldsymbol{q} := \begin{pmatrix} \rho \\ \rho v \\ E \end{pmatrix}, \quad \boldsymbol{G}(\boldsymbol{q}) := \begin{pmatrix} \rho v \\ \rho v^2 + w \\ v(E+p) \end{pmatrix}, \quad \boldsymbol{S}(\boldsymbol{q}) := \begin{pmatrix} 0 \\ 0 \\ -\rho v g \end{pmatrix},$$

where w is given by (1.8).

2.2.1 Well-Balanced Reconstruction

We now describe a special reconstruction, which is used to derive a well-balanced CU scheme. The main idea is to reconstruct equilibrium variables $(\rho, \rho v, w)$ rather than $(\rho, \rho v, E)$. For the first two components we still use formula (2.3) to obtain the same piecewise linear reconstructions as before, $\widetilde{\rho}(y)$ and $(\widetilde{\rho v})(y)$, and compute the corresponding point values of $\rho^{\mathrm{N,S}}$ and $(\rho v)^{\mathrm{N,S}}$, and then obtain $v^{\mathrm{N,S}} = (\rho v)^{\mathrm{N,S}}/\rho^{\mathrm{N,S}}$.

To reconstruct the third equilibrium variable w, we first compute the point values of R by integrating the piecewise linear reconstruction of ρ,

$$\widetilde{\rho}(y) = \sum_k \big(\overline{\rho}_k + (\rho_y)_k (y - y_k)\big) \cdot \chi_{C_k}(y),$$

which results in the piecewise quadratic approximation of R:

$$\widetilde{R}(y) = g \int\limits_{y_{k_L - \frac{1}{2}}}^{y} \widetilde{\rho}(\xi)\, d\xi = g \sum_k \left[\Delta y \sum_{i=k_L}^{k-1} \overline{\rho}_i + \overline{\rho}_k (y - y_{k-\frac{1}{2}}) + \frac{(\rho_y)_k}{2} (y - y_{k-\frac{1}{2}})(y - y_{k+\frac{1}{2}}) \right] \cdot \chi_{C_k}(y).$$

Then, the point values of R at the cell interfaces and cell centers are

$$R_{k+\frac{1}{2}} = g \Delta y \sum_{i=k_L}^{k} \overline{\rho}_i \quad \text{and} \quad R_k = g \Delta y \sum_{i=k_L}^{k-1} \overline{\rho}_i + \frac{g \Delta y}{2} \overline{\rho}_k - \frac{g (\Delta y)^2}{8} (\rho_y)_k, \tag{2.10}$$

respectively, and the values of w at the cell centers are set as

$$w_k = p_k + R_k, \tag{2.11}$$

where $p_k = (\gamma - 1) \left(\overline{E}_k - \frac{\overline{\rho}_k}{2} v_k^2 \right)$ is obtained from the corresponding EOS (1.5) and $v_k = (\overline{\rho v})_k / \overline{\rho}_k$.

Equipped with (2.11), we then apply the minmod reconstruction procedure to $\{w_k\}$ and obtain the point values of w at the cell interfaces:

$$w_k^{\rm N} = w_k + \frac{\Delta y}{2}(w_y)_k, \quad w_{k+1}^{\rm S} = w_{k+1} - \frac{\Delta y}{2}(w_y)_{k+1},$$

where

$$(w_y)_k = \text{minmod}\left(\theta\,\frac{w_{k+1}-w_k}{\Delta y},\ \frac{w_{k+1}-w_{k-1}}{2\Delta y},\ \theta\,\frac{w_k-w_{k-1}}{\Delta y}\right).$$

Finally, the point values of p and E needed for computation of numerical fluxes are

$$p_k^{\rm N} = w_k^{\rm N} - R_{k+\frac12}, \quad p_k^{\rm S} = w_k^{\rm S} - R_{k-\frac12}$$

and

$$E_k^{\rm N} = \frac{p_k^{\rm N}}{\gamma-1} + \frac{\left((\rho v)_k^{\rm N}\right)^2}{2\rho_k^{\rm N}}, \quad E_k^{\rm S} = \frac{p_k^{\rm S}}{\gamma-1} + \frac{\left((\rho v)_k^{\rm S}\right)^2}{2\rho_k^{\rm S}},$$

respectively.

Remark 2.1 In practice, it is convenient to compute the point values of $R_{k+\frac12}$ and R_k recursively, that is, replacing (2.10) with

$$R_{k_L-\frac12} = 0, \qquad \begin{cases} R_{k+\frac12} = R_{k-\frac12} + g\Delta y\,\bar\rho_k, \\ R_k = R_{k-\frac12} + \dfrac{g\Delta y}{2}\,\bar\rho_k - \dfrac{g(\Delta y)^2}{8}(\rho_y)_k, \end{cases} \quad k = k_L,\dots,k_R. \tag{2.12}$$

2.2.2 Well-Balanced Evolution

The cell-averages of $\bar{\boldsymbol{q}}$ are evolved in time according to the following system of ODEs:

$$\frac{d}{dt}\bar{\boldsymbol{q}}_k = -\frac{\boldsymbol{\mathcal{G}}_{k+\frac12} - \boldsymbol{\mathcal{G}}_{k-\frac12}}{\Delta y} + \overline{\boldsymbol{S}}_k. \tag{2.13}$$

Here, the second and third components of the numerical fluxes $\boldsymbol{\mathcal{G}}$ are computed the same way as in (2.2):

$$\mathcal{G}^{(2)}_{k+\frac12} := \frac{b^+_{k+\frac12}\left(\rho_k^{\rm N}(v_k^{\rm N})^2 + w_k^{\rm N}\right) - b^-_{k+\frac12}\left(\rho_{k+1}^{\rm S}(v_{k+1}^{\rm S})^2 + w_{k+1}^{\rm S}\right)}{b^+_{k+\frac12} - b^-_{k+\frac12}} + \beta_{k+\frac12}\left((\rho v)_{k+1}^{\rm S} - (\rho v)_k^{\rm N}\right), \tag{2.14}$$

$$\mathcal{G}^{(3)}_{k+\frac12} := \frac{b^+_{k+\frac12}v_k^{\rm N}(E_k^{\rm N}+p_k^{\rm N}) - b^-_{k+\frac12}v_{k+1}^{\rm S}(E_{k+1}^{\rm S}+p_{k+1}^{\rm S})}{b^+_{k+\frac12} - b^-_{k+\frac12}} + \beta_{k+\frac12}\left(E_{k+1}^{\rm S} - E_k^{\rm N}\right), \tag{2.15}$$

while the first component should be modified in order to preserve the steady state (1.10):

$$\mathcal{G}^{(1)}_{k+\frac12} = \frac{b^+_{k+\frac12}(\rho v)_k^{\rm N} - b^-_{k+\frac12}(\rho v)_{k+1}^{\rm S}}{b^+_{k+\frac12} - b^-_{k+\frac12}} + \beta_{k+\frac12}H\left(\frac{|w_{k+1}-w_k|}{\Delta y}\cdot\frac{y_{k_R+\frac12}-y_{k_L-\frac12}}{\max_k\{w_k\}}\right)\left(\rho_{k+1}^{\rm S} - \rho_k^{\rm N}\right). \tag{2.16}$$

Notice that the last term in (2.16) is now multiplied by a smooth function H, designed to be very small when the computed solution is locally (almost) at steady state, that is, at the cell interfaces where $\frac{|w_{k+1}-w_k|}{\Delta y} \sim 0$, and to be very close to 1 elsewhere. This is done in order to guarantee the well-balanced property of the scheme as we show in Theorem 2.1 proved in §2.2.3. On the other hand, the modification of the original CU flux is quite minor since $H(\psi)$ is very close to 1 unless ψ is very small.

A sketch of a typical function H is shown in Figure 2.1. In all of our numerical experiments, we have used

$$H(\psi) = \frac{(C\psi)^m}{1+(C\psi)^m}, \tag{2.17}$$

with $C = 200$ and $m = 6$. To reduce the dependence of the computed solution on the choice of particular values of C and m, the argument of H in (2.16) is normalized by a factor $\frac{y_{k_R+\frac{1}{2}}-y_{k_L-\frac{1}{2}}}{\max_k\{w_k\}}$, which makes $H(\psi)$ dimensionless.

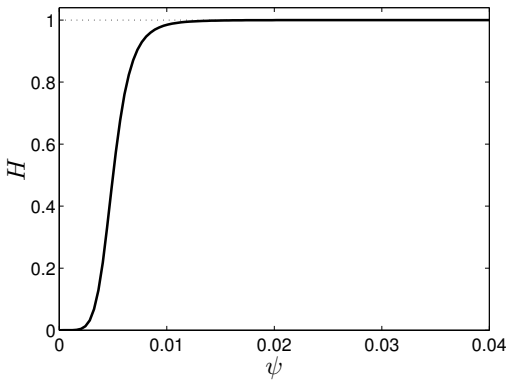

Figure 2.1: Sketch of $H(\psi)$.

Finally, the cell averages of the source term are approximated using the midpoint quadrature rule as follows:

$$\overline{\boldsymbol{S}}_k = (0, 0, -g(\overline{\rho v})_k)^T. \tag{2.18}$$

2.2.3 Proof of the Well-Balanced Property

Theorem 2.1 *The semi-discrete CU scheme (2.13)–(2.18) coupled with the reconstruction described in §2.2.1 is well-balanced in the sense that it preserves the steady state (1.10).*

Proof: Assume that at certain time level, we have

$$v_k^{\rm N} \equiv v_k \equiv v_k^{\rm S} \equiv 0 \quad \text{and} \quad w_k^{\rm N} \equiv w_k \equiv w_k^{\rm S} \equiv \widehat{w}, \tag{2.19}$$

where $\widehat{w}$ is a constant. To show that the proposed scheme is well-balanced, we need to show that the right-hand side (RHS) of (2.13) is identically equal to zero for the data in (2.19). Since the source term (2.18) vanishes for $v_k = 0$, it is enough to prove that the numerical fluxes are constant for the data in (2.19).

Indeed, the first components of the numerical flux, (2.16), vanish since $v_k^{\rm N} = v_{k+1}^{\rm S} = 0$ and $w_k = w_{k+1} = \widehat{w}$ (the latter implies $H\left(\frac{|w_{k+1}-w_k|}{\Delta y} \cdot \frac{y_{k_R+\frac{1}{2}}-y_{k_L-\frac{1}{2}}}{\max_k w_k}\right) = H(0) = 0$). The second

components of the numerical flux, (2.14), are constant and equal to $\widehat{w}$ since $v^{\rm N}_k = v^{\rm S}_{k+1} = 0$ and $w^{\rm N}_k = w^{\rm S}_{k+1} = \widehat{w}$. Finally, the third components of the numerical flux, (2.15), also vanish:

$$\mathcal{G}^{(3)}_{k+\frac12} = \beta_{k+\frac12}\left(E^{\rm S}_{k+1} - E^{\rm N}_k\right) = \frac{\beta_{k+\frac12}}{\gamma-1}\left(p^{\rm S}_{k+1} - p^{\rm N}_k\right) = \frac{\beta_{k+\frac12}}{\gamma-1}\left[\left(w^{\rm S}_{k+1} - R_{k+\frac12}\right) - \left(w^{\rm N}_k - R_{k+\frac12}\right)\right] = 0,$$

since $w^N_k = w^S_{k+1} = \widehat{w}$. ■

3 Two-Dimensional Numerical Method

In this section, we describe the well-balanced semi-discrete CU scheme for the 2-D Euler equations with gravitation. Similarly to the 1-D case, we rewrite the system (1.1)–(1.5) as follows:

$$\begin{cases} \rho_t + (\rho u)_x + (\rho v)_y = 0,\\ (\rho u)_t + (\rho u^2 + p)_x + (\rho uv)_y = 0,\\ (\rho v)_t + (\rho uv)_x + (\rho v^2 + w)_y = 0,\\ E_t + (u(E+p))_x + (v(E+p))_y = -\rho v g. \end{cases} \tag{3.1}$$

This system can also be written in the vector form (1.1) with

$$\boldsymbol{q} := \begin{pmatrix} \rho\\ \rho u\\ \rho v\\ E \end{pmatrix}, \quad \boldsymbol{F}(\boldsymbol{q}) := \begin{pmatrix} \rho u\\ \rho u^2 + p\\ \rho uv\\ u(E+p) \end{pmatrix}, \quad \boldsymbol{G}(\boldsymbol{q}) := \begin{pmatrix} \rho v\\ \rho uv\\ \rho v^2 + w\\ v(E+p) \end{pmatrix}, \quad \boldsymbol{S}(\boldsymbol{q}) := \begin{pmatrix} 0\\ 0\\ 0\\ -\rho v g \end{pmatrix},$$

where

$$w := p + R, \quad R(x,y,t) := g\int\limits_y^{\infty} \rho(x,\xi,t)\,d\xi. \tag{3.2}$$

3.1 Well-Balanced Central-Upwind Scheme

We consider a rectangular computational domain and partition it into the uniform Cartesian cells $C_{j,k} := [x_{j-\frac12}, x_{j+\frac12}] \times [y_{k-\frac12}, y_{k+\frac12}]$ of size $|C_{j,k}| = \Delta x\Delta y$ centered at $(x_j, y_k) = (j\Delta x, k\Delta y)$, $j = j_L, \ldots, j_R$, $k = k_L, \ldots, k_R$. Similarly to the 1-D case, we assume that at a certain time level t, the cell averages of the computed numerical solution,

$$\overline{\boldsymbol{q}}_{j,k}(t) := \frac{1}{\Delta x}\frac{1}{\Delta y}\iint\limits_{C_{j,k}} \boldsymbol{q}(x,y,t)\,dx\,dy, \tag{3.3}$$

are available.

3.1.1 Well-Balanced Reconstruction

Similarly to the 1-D case, we reconstruct only the first three components of the conservative variables $\boldsymbol{q}$ (ρ, ρu and ρv):

$$\widetilde{q}^{(i)}(x,y)=\bar{q}^{(i)}_{j,k}+(q^{(i)}_x)_{j,k}(x-x_j)+(q^{(i)}_y)_{j,k}(y-y_k),\quad (x,y)\in C_{j,k},\quad i=1,2,3, \tag{3.4}$$

and compute the corresponding point values at the cell interfaces $(x_{j\pm\frac12},y_k)$ and $(x_j,y_{k\pm\frac12})$:

$$\begin{aligned}
&(q^{(i)})^{\rm E}_{j,k}:=\widetilde{q}^{(i)}(x_{j+\frac12}-0,y_k)=\bar{q}^{(i)}_{j,k}+\frac{\Delta x}{2}(q^{(i)}_x)_{j,k},\\
&(q^{(i)})^{\rm W}_{j,k}:=\widetilde{q}^{(i)}(x_{j-\frac12}+0,y_k)=\bar{q}^{(i)}_{j,k}-\frac{\Delta x}{2}(q^{(i)}_x)_{j,k},\\
&(q^{(i)})^{\rm N}_{j,k}:=\widetilde{q}^{(i)}(x_j,y_{k+\frac12}-0)=\bar{q}^{(i)}_{j,k}+\frac{\Delta y}{2}(q^{(i)}_y)_{j,k},\\
&(q^{(i)})^{\rm S}_{j,k}:=\widetilde{q}^{(i)}(x_j,y_{k-\frac12}+0)=\bar{q}^{(i)}_{j,k}-\frac{\Delta y}{2}(q^{(i)}_y)_{j,k},
\end{aligned}\qquad i=1,2,3,$$

where the slopes $(q^{(i)}_x)_{j,k}$ and $(q^{(i)}_y)_{j,k}$ are computed using a nonlinear limiter, for example, the generalized minmod limiter:

$$\begin{aligned}
(q^{(i)}_x)_{j,k}&={\rm minmod}\left(\theta\,\frac{\bar{q}^{(i)}_{j+1,k}-\bar{q}^{(i)}_{j,k}}{\Delta x},\ \frac{\bar{q}^{(i)}_{j+1,k}-\bar{q}^{(i)}_{j-1,k}}{2\Delta x},\ \theta\,\frac{\bar{q}^{(i)}_{j,k}-\bar{q}^{(i)}_{j-1,k}}{\Delta x}\right),\\
(q^{(i)}_y)_{j,k}&={\rm minmod}\left(\theta\,\frac{\bar{q}^{(i)}_{j,k+1}-\bar{q}^{(i)}_{j,k}}{\Delta y},\ \frac{\bar{q}^{(i)}_{j,k+1}-\bar{q}^{(i)}_{j,k-1}}{2\Delta y},\ \theta\,\frac{\bar{q}^{(i)}_{j,k}-\bar{q}^{(i)}_{j,k-1}}{\Delta y}\right),
\end{aligned}\qquad i=1,2,3.$$

We then estimate the one-sided local speeds of propagation in the x- and y- directions, respectively, using the smallest and largest eigenvalues of the Jacobians $\frac{\partial \boldsymbol{F}}{\partial \boldsymbol{q}}$ and $\frac{\partial \boldsymbol{G}}{\partial \boldsymbol{q}}$:

$$\begin{aligned}
&a^+_{j+\frac12,k}=\max\left(u^{\rm E}_{j,k}+c^{\rm E}_{j,k},\,u^{\rm W}_{j+1,k}+c^{\rm W}_{j+1,k},\,0\right),\qquad a^-_{j+\frac12,k}=\min\left(u^{\rm E}_{j,k}-c^{\rm E}_{j,k},\,u^{\rm W}_{j+1,k}-c^{\rm W}_{j+1,k},\,0\right),\\
&b^+_{j,k+\frac12}=\max\left(v^{\rm N}_{j,k}+c^{\rm N}_{j,k},\,v^{\rm S}_{j,k+1}+c^{\rm S}_{j,k+1},\,0\right),\qquad b^-_{j,k+\frac12}=\min\left(v^{\rm N}_{j,k}-c^{\rm N}_{j,k},\,v^{\rm S}_{j,k+1}-c^{\rm S}_{j,k+1},\,0\right),
\end{aligned}$$

where the velocities $u^{\rm E}_{j,k},u^{\rm W}_{j+1,k},v^{\rm N}_{j,k}$ and $v^{\rm S}_{j,k+1}$ are obtained from the identities $u\equiv(\rho u)/\rho$ and $v\equiv(\rho v)/\rho$ and the speeds of sound $c^{\rm E}_{j,k},c^{\rm W}_{j+1,k},c^{\rm N}_{j,k}$ and $c^{\rm S}_{j,k+1}$ are computed from the definition $c^2=\gamma p/\rho$.

The calculation of the point values for the forth conservative variable E requires a special treatment, which is different in the horizontal (x) and vertical (y) directions.

In the x-direction, we first compute the point values of p at the cell centers using the EOS (1.5):

$$p_{j,k}=(\gamma-1)\left(\overline{E}_{j,k}-\frac{(\overline{\rho u})^2_{j,k}+(\overline{\rho v})^2_{j,k}}{2\bar{\rho}_{j,k}}\right),$$

and then compute the cell interface values of p using a nonlinear limiter, for example, the generalized minmod one:

$$p^{\rm E}_{j,k}=p_{j,k}+\frac{\Delta x}{2}(p_x)_{j,k},\quad p^{\rm W}_{j,k}=p_{j,k}-\frac{\Delta x}{2}(p_x)_{j,k},$$

where

$$(p_x)_{j,k}=\text{minmod}\left(\theta\,\frac{p_{j+1,k}-p_{j,k}}{\Delta x},\ \frac{p_{j+1,k}-p_{j-1,k}}{2\Delta x},\ \theta\,\frac{p_{j,k}-p_{j-1,k}}{\Delta x}\right).$$

Equipped with these values, we then compute the required cell interface values of E:

$$E^{\rm E}_{j,k}=\frac{p^{\rm E}_{j,k}}{\gamma-1}+\frac{\rho^{\rm E}_{j,k}}{2}\left(\left(u^{\rm E}_{j,k}\right)^2+\left(v^{\rm E}_{j,k}\right)^2\right),\quad E^{\rm W}_{j,k}=\frac{p^{\rm W}_{j,k}}{\gamma-1}+\frac{\rho^{\rm W}_{j,k}}{2}\left(\left(u^{\rm W}_{j,k}\right)^2+\left(v^{\rm W}_{j,k}\right)^2\right).$$

Remark 3.1 As an alternative approach, one can compute the point values $E^{\rm E}_{j,k}$ and $E^{\rm W}_{j,k}$ using a piecewise linear reconstruction of the conservative variable E rather than p and still obtain a well-balanced reconstruction. However, our numerical experiments (not reported in this paper for the sake of brevity) indicate that reconstructing E in the x-direction leads to the loss of symmetry in the computed solution.

In the y-direction, we follow the same idea as in the 1-D case. First, we compute the values of R at the cell interfaces and cell centers in a complete analogy with (2.12):

$$R_{j,k_L-\frac12}=0,\qquad\begin{cases}R_{j,k+\frac12}=R_{j,k-\frac12}+g\Delta y\bar\rho_{j,k},\\ R_{j,k}=R_{j,k-\frac12}+\dfrac{g\Delta y}{2}\bar\rho_{j,k}-\dfrac{g(\Delta y)^2}{8}(\rho_y)_{j,k},\end{cases}\qquad j=j_L,\ldots,j_R,\ k=k_L,\ldots,k_R.$$

We then compute $w_{j,k}$ as follows:

$$w_{j,k}=p_{j,k}+R_{j,k}.$$

Next, reconstructing w in the y-direction yields

$$w^{\rm N}_{j,k}=w_{j,k}+\frac{\Delta y}{2}(w_y)_{j,k},\quad w^{\rm S}_{j,k}=w_{j,k}-\frac{\Delta y}{2}(w_y)_{j,k},$$

where

$$(w_y)_{j,k}=\text{minmod}\left(\theta\,\frac{w_{j,k+1}-w_{j,k}}{\Delta y},\ \frac{w_{j,k+1}-w_{j,k-1}}{2\Delta y},\ \theta\,\frac{w_{j,k}-w_{j,k-1}}{\Delta y}\right).$$

Finally, the obtained point values of w are used to evaluate the corresponding point values p from (3.2):

$$p^{\rm N}_{j,k}=w^{\rm N}_{j,k}-R_{j,k+\frac12},\quad p^{\rm S}_{j,k}=w^{\rm S}_{j,k}-R_{j,k-\frac12},$$

and E from (1.5):

$$E^{\rm N}_{j,k}=\frac{p^{\rm N}_{j,k}}{\gamma-1}+\frac{\left((\rho u)^{\rm N}_{j,k}\right)^2+\left((\rho v)^{\rm N}_{j,k}\right)^2}{2\rho^{\rm N}_{j,k}},\quad E^{\rm S}_{j,k}=\frac{p^{\rm S}_{j,k}}{\gamma-1}+\frac{\left((\rho u)^{\rm S}_{j,k}\right)^2+\left((\rho v)^{\rm S}_{j,k}\right)^2}{2\rho^{\rm S}_{j,k}}.$$

3.1.2 Well-Balanced Evolution

The cell-averages of $\bar{\boldsymbol{q}}$ are evolved in time according to the following system of ODEs:

$$\frac{d}{dt}\bar{\boldsymbol{q}}_{j,k}=-\frac{\boldsymbol{\mathcal{F}}_{j+\frac12,k}-\boldsymbol{\mathcal{F}}_{j-\frac12,k}}{\Delta x}-\frac{\boldsymbol{\mathcal{G}}_{j,k+\frac12}-\boldsymbol{\mathcal{G}}_{j,k-\frac12}}{\Delta y}+\overline{\boldsymbol{S}}_{j,k}.\tag{3.5}$$

Here, $\boldsymbol{\mathcal{F}}$ and $\boldsymbol{\mathcal{G}}$ are numerical fluxes. Introducing the notations

$$\alpha_{j+\frac12,k}:=\frac{a^+_{j+\frac12,k}a^-_{j+\frac12,k}}{a^+_{j+\frac12,k}-a^-_{j+\frac12,k}}\quad\text{and}\quad\beta_{j,k+\frac12}:=\frac{b^+_{j,k+\frac12}b^-_{j,k+\frac12}}{b^+_{j,k+\frac12}-b^-_{j,k+\frac12}},$$

we write the components of $\boldsymbol{\mathcal{F}}$ and $\boldsymbol{\mathcal{G}}$ as

$$\begin{aligned}
\mathcal{F}^{(1)}_{j+\frac12,k}=&\frac{a^+_{j+\frac12,k}(\rho u)^{\rm E}_{j,k}-a^-_{j+\frac12,k}(\rho u)^{\rm W}_{j+1,k}}{a^+_{j+\frac12,k}-a^-_{j+\frac12,k}}\\
&+\alpha_{j+\frac12,k}H\left(\frac{|w_{j+1,k}-w_{j,k}|}{\Delta x}\cdot\frac{x_{k_R+\frac12}-x_{k_L-\frac12}}{\max_{j,k}\{w_{j,k}\}}\right)\left(\rho^{\rm W}_{j+1,k}-\rho^{\rm E}_{j,k}\right),\\
\mathcal{F}^{(2)}_{j+\frac12,k}=&\frac{a^+_{j+\frac12,k}\left(\rho^{\rm E}_{j,k}(u^{\rm E}_{j,k})^2+p^{\rm E}_{j,k}\right)-a^-_{j+\frac12,k}(\rho^{\rm W}_{j+1,k}(u^{\rm W}_{j+1,k})^2+p^{\rm W}_{j+1,k})}{a^+_{j+\frac12,k}-a^-_{j+\frac12,k}}\\
&+\alpha_{j+\frac12,k}\left((\rho u)^{\rm W}_{j+1,k}-(\rho u)^{\rm E}_{j,k}\right),\\
\mathcal{F}^{(3)}_{j+\frac12,k}=&\frac{a^+_{j+\frac12,k}\rho^{\rm E}_{j,k}u^{\rm E}_{j,k}v^{\rm E}_{j,k}-a^-_{j+\frac12,k}\rho^{\rm W}_{j+1,k}u^{\rm W}_{j+1,k}v^{\rm W}_{j+1,k}}{a^+_{j+\frac12,k}-a^-_{j+\frac12,k}}+\alpha_{j+\frac12,k}\left((\rho v)^{\rm W}_{j+1,k}-(\rho v)^{\rm E}_{j,k}\right),\\
\mathcal{F}^{(4)}_{j+\frac12,k}=&\frac{a^+_{j+\frac12,k}u^{\rm E}_{j,k}(E^{\rm E}_{j,k}+p^{\rm E}_{j,k})-a^-_{j+\frac12,k}u^{\rm W}_{j+1,k}(E^{\rm W}_{j+1,k}+p^{\rm W}_{j+1,k})}{a^+_{j+\frac12,k}-a^-_{j+\frac12,k}}+\alpha_{j+\frac12,k}\left(E^{\rm W}_{j+1,k}-E^{\rm E}_{j,k}\right),\\
\mathcal{G}^{(1)}_{j,k+\frac12}=&\frac{b^+_{j,k+\frac12}(\rho v)^{\rm N}_{j,k}-b^-_{j,k+\frac12}(\rho v)^{\rm S}_{j,k+1}}{b^+_{j,k+\frac12}-b^-_{j,k+\frac12}}\\
&+\beta_{j,k+\frac12}H\left(\frac{|w_{j,k+1}-w_{j,k}|}{\Delta y}\cdot\frac{y_{k_R+\frac12}-y_{k_L-\frac12}}{\max_{j,k}\{w_{j,k}\}}\right)\left(\rho^{\rm S}_{j,k+1}-\rho^{\rm N}_{j,k}\right),\\
\mathcal{G}^{(2)}_{j,k+\frac12}=&\frac{b^+_{j,k+\frac12}\rho^{\rm N}_{j,k}u^{\rm N}_{j,k}v^{\rm N}_{j,k}-b^-_{j,k+\frac12}\rho^{\rm S}_{j,k+1}u^{\rm S}_{j,k+1}v^{\rm S}_{j,k+1}}{b^+_{j,k+\frac12}-b^-_{j,k+\frac12}}+\beta_{j,k+\frac12}\left((\rho u)^{\rm S}_{j,k+1}-(\rho u)^{\rm N}_{j,k}\right),\\
\mathcal{G}^{(3)}_{j,k+\frac12}=&\frac{b^+_{j,k+\frac12}\left(\rho^{\rm N}_{j,k}(v^{\rm N}_{j,k})^2+w^{\rm N}_{j,k}\right)-b^-_{j,k+\frac12}\left(\rho^{\rm S}_{j,k+1}(v^{\rm S}_{j,k+1})^2+w^{\rm S}_{j,k+1}\right)}{b^+_{j,k+\frac12}-b^-_{j,k+\frac12}}\\
&+\beta_{j,k+\frac12}\left((\rho v)^{\rm S}_{j,k+1}-(\rho v)^{\rm N}_{j,k}\right),\\
\mathcal{G}^{(4)}_{j,k+\frac12}=&\frac{b^+_{j,k+\frac12}v^{\rm N}_{j,k}(E^{\rm N}_{j,k}+p^{\rm N}_{j,k})-b^-_{j,k+\frac12}v^{\rm S}_{j,k+1}(E^{\rm S}_{j,k+1}+p^{\rm S}_{j,k+1})}{b^+_{j,k+\frac12}-b^-_{j,k+\frac12}}+\beta_{j,k+\frac12}\left(E^{\rm S}_{j,k+1}-E^{\rm N}_{j,k}\right),
\end{aligned}$$

where the function H in the first components of the x and y numerical fluxes is as before defined in (2.17). The cell averages of the source term in (3.5) are approximated using the midpoint quadrature rule as follows:

$$\overline{\boldsymbol{S}}_{j,k}=(0,0,0,-g(\overline{\rho v})_{j,k})^T.$$

Finally, we state the following well-balanced property of the proposed 2-D CU scheme.

Theorem 3.1 *The 2-D semi-discrete CU scheme described in §3.1.1 and §3.1.2 above is well-balanced in the sense that it preserves the steady state (1.11).*

Proof: The proof is similar to the proof of Theorem 2.1. ■

4 Numerical Examples

In this section, we present a number of 1-D and 2-D numerical examples, in which we demonstrate the performance of the proposed well-balanced semi-discrete CU scheme.

In all of the examples below, we have used a third-order strong stability preserving (SSP) Runge-Kutta method (see, e.g., [12, 13, 32]) to solve the ODE systems (2.13) and (3.5). The CFL number has been set to 0.4. Also, we have used the following constant values: the minmod parameter $\theta = 1.3$ and the specific heat ratio $\gamma = 1.4$.

4.1 One-Dimensional Examples

Example 1—Shock Tube Problem. The first example is a modification of the Sod shock tube problem taken from [26, 36]. We solve the 1-D system (1.6), (1.7) with $g = 1$ in the computational domain $[0, 1]$ using the following initial data:

$$(\rho(y,0), v(y,0), p(y,0)) = \begin{cases} (1,0,1), & \text{if } y \le 0.5, \\ (0.125,0,0.1), & \text{if } y > 0.5, \end{cases}$$

and reflecting boundary conditions at the both ends of the computational domain. These boundary conditions are implemented using the ghost cell technique as follows:

$$\begin{aligned} &\bar{\rho}_{k_L-1} := \bar{\rho}_{k_L}, \quad v_{k_L-1} := -v_{k_L}, \quad w_{k_L-1} := w_{k_L}, \\ &\bar{\rho}_{k_R+1} := \bar{\rho}_{k_R}, \quad v_{k_R+1} := -v_{k_R}, \quad w_{k_R+1} := w_{k_R}, \end{aligned}$$

where $N := k_R - k_L + 1$ is a total number of grid cells.

We compute the solution using $N = 100$ uniformly placed grid cells and compare it with the reference solution obtained using $N = 2000$ uniform cells. In Figure 4.1, we plot both the coarse and fine grid solutions at time $T = 0.2$. As one can see, the proposed CU scheme captures the solutions on coarse mesh quite well showing a good agreement with both the reference solution and the results obtained in [26, 36].

Example 2—Isothermal Equilibrium Solution. In the second example, taken from [36] (see also [24, 26, 34]), we test the ability of the proposed CU scheme to accurately capture small perturbations of the steady state

$$\rho(y) = e^{-y}, \quad v(y) \equiv 0, \quad p(y) = ge^{-y}, \tag{4.1}$$

which satisfies (1.10).

We take the computational domain $[0, 1]$ and use a zero-order extrapolation at the boundaries:

$$\begin{aligned} &\bar{\rho}_{k_L-1} := \bar{\rho}_{k_L}, \quad v_{k_L-1} := v_{k_L}, \quad w_{k_L-1} := w_{k_L}, \\ &\bar{\rho}_{k_R+1} := \bar{\rho}_{k_R}, \quad v_{k_R+1} := v_{k_R}, \quad w_{k_R+1} := w_{k_R}. \end{aligned}$$

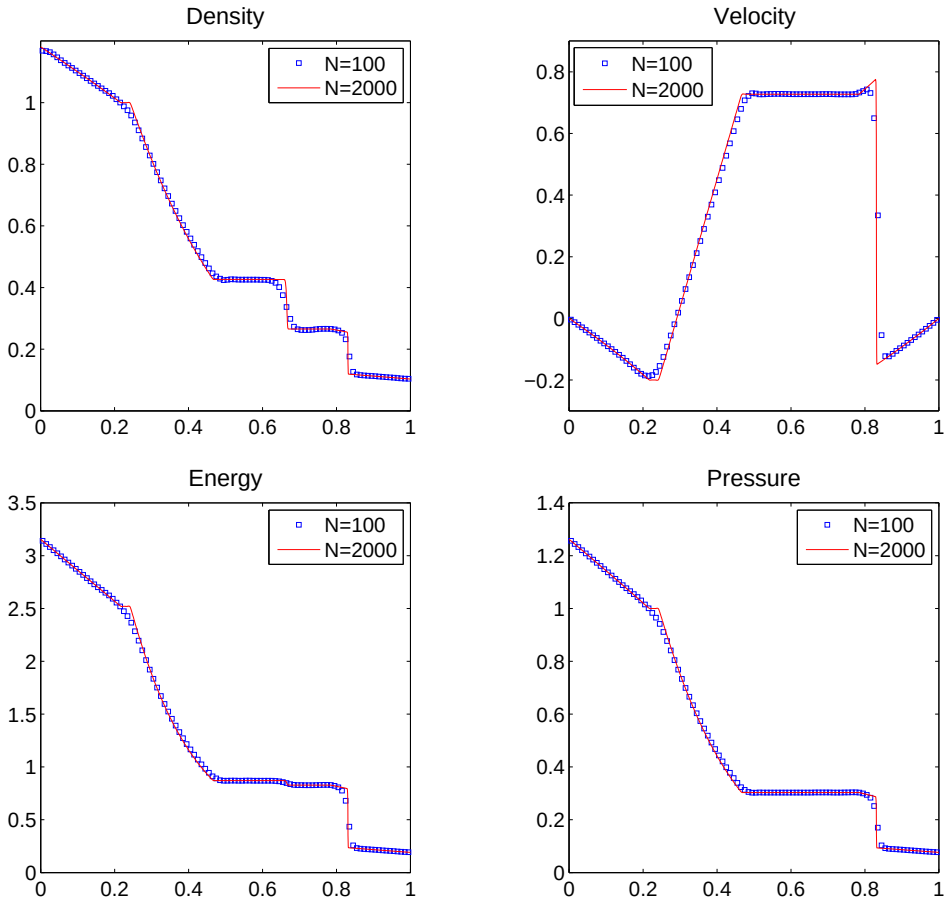

Figure 4.1: Example 1: Solution ($\rho(y,0.2)$, $v(y,0.2)$, $E(y,0.2)$ and $p(y,0.2)$) computed using $N=100$ and $N=2000$ cells.

Note that the boundary conditions on w can be recast in terms of p and ρ as

$$p_{k_L-1}=p_{k_L}+g\Delta y\bar{\rho}_{k_L},\quad p_{k_R+1}=p_{k_R}-g\Delta y\bar{\rho}_{k_R}.$$

We first numerically verify the well-balanced property of the proposed CU scheme by solving the 1-D system (1.6), (1.7) with $g=1$ subject to the initial conditions corresponding to the steady state (4.1). We use several uniform grids and observe that the initial conditions are preserved within the machine accuracy.

Next, we introduce a small initial pressure perturbation and consider the system (1.6), (1.7) subject to the following initial data:

$$\rho(y,0)=e^{-y},\quad v(y,0)\equiv 0,\quad p(y,0)=ge^{-y}+\eta e^{-100(y-0.5)^2},$$

where η is a small positive number. In the numerical experiments, we use larger ($\eta=10^{-2}$) and smaller ($\eta=10^{-4}$) perturbations.

We first apply the proposed well-balanced CU scheme to this problem and compute the solution at time $T=0.25$. The obtained pressure perturbation ($p(y,0.25)-ge^{-y}$) computed using $N=200$ and $N=2000$ (reference solution) uniform grid cells are plotted in Figure 4.2 for both $\eta=10^{-2}$ and $\eta=10^{-4}$. As one can see, the scheme accurately captures both small

and large perturbations on a relatively coarse mesh with $N = 200$. In order to demonstrate the importance of the well-balanced property, we apply the non-well-balanced CU scheme described in §2.1 to the same initial-boundary value problem. The obtained results are shown in Figure 4.2 as well. It should be observed that while the larger perturbation is quite accurately computed by both schemes, the non-well-balanced CU scheme fails to capture the smaller one.

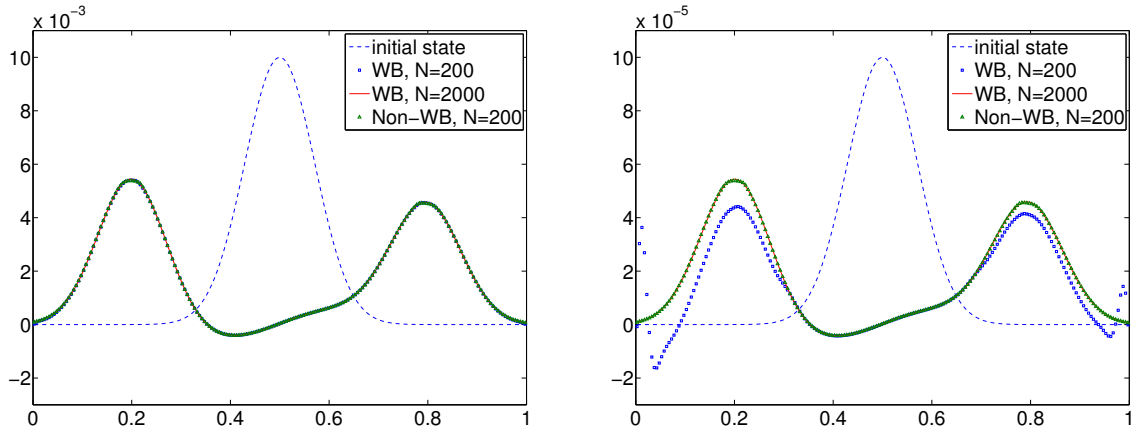

Figure 4.2: Example 2: Pressure perturbation ($p(y, 0.25) - ge^{-y}$) computed by the well-balanced (WB) and non-well-balanced (Non-WB) CU schemes with $N = 200$ and $N = 2000$ for $\eta = 10^{-2}$ (left) and $\eta = 10^{-4}$ (right).

4.2 Two-Dimensional Examples

Example 3—Isothermal Equilibrium Solution. The first 2-D example was studied in [36]. We consider the system (3.1), (3.2) with $g = 1$ subject to the initial data that are in an isothermal equilibrium:

$$\rho(x, y, 0) = \rho_0 e^{-\frac{\rho_0 g y}{p_0}}, \quad p(x, y, 0) = p_0 e^{-\frac{\rho_0 g y}{p_0}}, \quad u(x, y, 0) \equiv v(x, y, 0) \equiv 0, \tag{4.2}$$

where $\rho_0 = 1.21$ and $p_0 = 1$, and the solid wall boundary conditions imposed at the edges of the unit square $[0, 1] \times [0, 1]$.

We compute the solution until the final time $T = 1$ using the proposed well-balanced CU scheme on 50×50, 100×100 and 200×200 uniform cells. On all of these grids, the initial data are preserved within the machine accuracy. On contrary, the non-well-balanced CU scheme preserves the initial equilibrium within the accuracy of the scheme only, as can be seen in Table 4.1, where we present the L^1-errors for both ρ, ρu, ρv and E components of the non-well-balanced solution.

Next, we add a small perturbation to the initial pressure (compare with (4.2)):

$$p(x, y, 0) = p_0 e^{-\frac{\rho_0 g y}{p_0}} + \eta e^{-\frac{100\rho_0 g}{p_0}\left((x-0.3)^2+(y-0.3)^2\right)}, \quad \eta = 10^{-3}.$$

In Figures 4.3 and 4.4 (upper row), we plot the pressure computed by both the well-balanced and non-well-balanced CU schemes at time $T = 0.15$ using 50×50 uniform cells. As one can clearly see, the well-balanced CU scheme can capture the small pressure perturbation much

$N \times N$	ρ	ρu	ρv	E
50 × 50	1.05E-03	0.00E+00	5.72E-05	9.61E-05
100 × 100	4.02E-04	0.00E+00	2.07E-05	4.10E-05
200 × 200	1.63E-04	0.00E+00	7.11E-06	1.57E-05

Table 4.1: Example 3: L^1-errors for the non-well-balanced CU scheme.

more accurately than the non-well-balanced one. When the mesh is refined to 200 × 200 uniform cells, the non-well-balanced solution becomes better, but still less accurate than the well-balanced one, see Figure 4.4 (lower row).

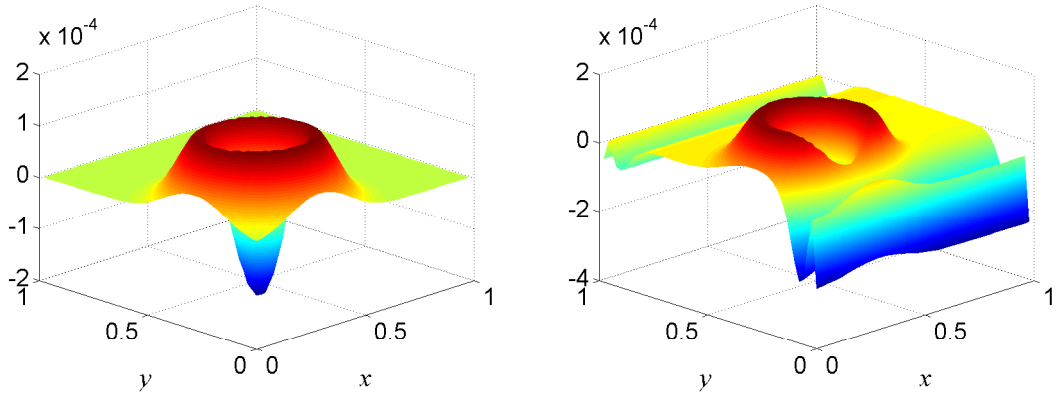

Figure 4.3: Example 3: Pressure perturbation computed by the well-balanced (left) and non-well-balanced (right) CU schemes using 50 × 50 uniform cells.

Example 4—Explosion. In the second 2-D example, we compare the performance of well-balanced and non-well-balanced CU schemes in an explosion setting and demonstrate nonphysical shock waves generated by non-well-balanced scheme.

We solve the system (3.1), (3.2) with $g = 0.118$ in the computational domain $[0, 3] \times [0, 3]$, subject to the following initial data:

$$\rho(x, y, 0) \equiv 1, \quad u(x, y, 0) \equiv 0, \quad p(x, y, 0) = 1 - gy + \begin{cases} 0.005, & (x - 1.5)^2 + (y - 1.5)^2 < 0.01, \\ 0, & \text{otherwise.} \end{cases}$$

Zero-order extrapolation is used as the boundary conditions in all of the directions.

We use a uniform grid with 101 × 101 cells and compute the solution by both the well-balanced and non-well-balanced CU schemes until the final time $T = 2.4$. At first, a circular shock wave is developed and later on it transmits through the boundary. Due to the heat generated by the explosion, the gas at the center expands and its density decreases generating a positive vertical momentum at the center of the domain. In Figures 4.5 and 4.6, we plot the solution (ρ and $\sqrt{u^2 + v^2}$ at times $t = 1.2$, 1.8 and 2.4) computed by the well-balanced and non-well-balanced schemes, respectively. As one can see, the well-balanced scheme accurately

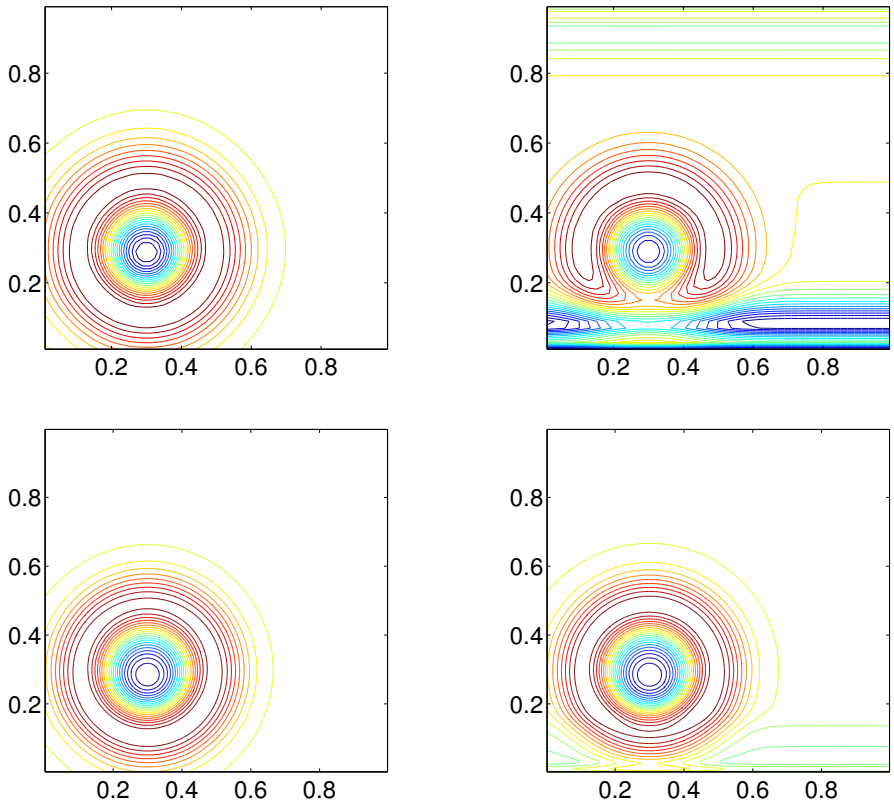

Figure 4.4: Example 3: Contour plot of the pressure perturbation computed by well-balanced (left column) and non-well-balanced (right column) CU schemes using 50×50 (upper row) and 200×200 (lower row) uniform cells.

captures the behavior of the solution at all stages, while the non-well-balanced scheme produces significant oscillations at the smaller time $t = 1.2$, which totally dominate the solution, especially its velocity field, by the final time $T = 2.4$.

Acknowledgment: The work of A. Chertock was supported in part by the NSF Grants DMS-1115682 and DMS-1216974 and the ONR Grant N00014-12-1-0832. The work of Shumo Cui was supported in part by the NSF Grants DMS-1115718 and DMS-1216957. The work of A. Kurganov was supported in part by the NSF Grant DMS-1115718 and DMS-1216957 and the ONR Grant N00014-12-1-0833. The work of Ş. N. Özcan was supported in part by the Turkish Ministry of National Education. The work of E. Tadmor was supported in part by the ONR grant N00014-12-1-0318 and the NSF grant DMS-1008397.

References

[1] E. AUDUSSE, F. BOUCHUT, M.-O. BRISTEAU, R. KLEIN, AND B. PERTHAME, *A fast and stable well-balanced scheme with hydrostatic reconstruction for shallow water flows*, SIAM J. Sci. Comput., 25 (2004), pp. 2050–2065.

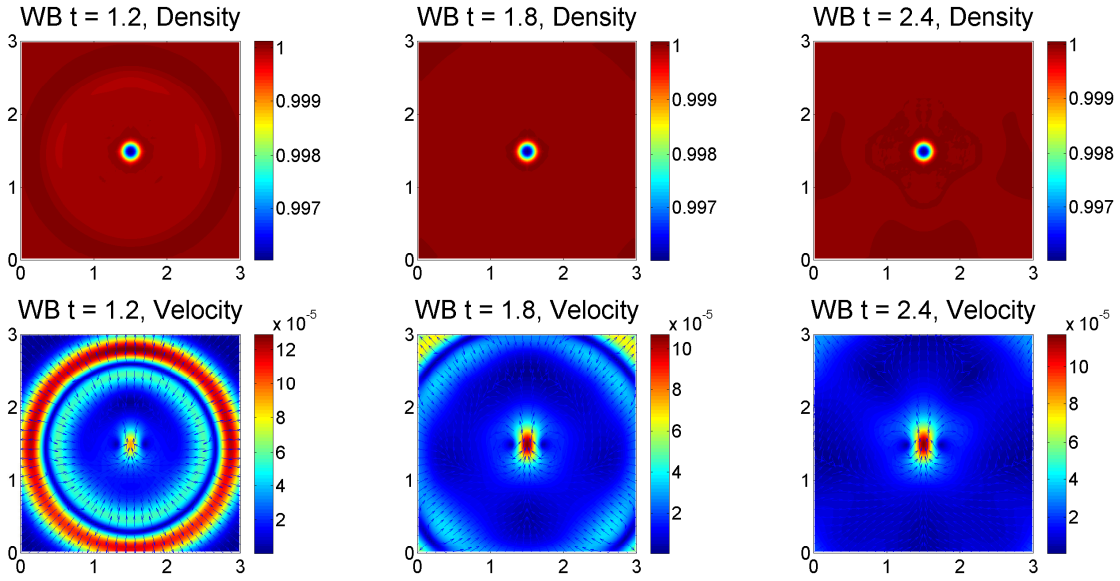

Figure 4.5: Example 4: Density (ρ) and velocity ($\sqrt{u^2+v^2}$) computed by the well-balanced CU scheme.

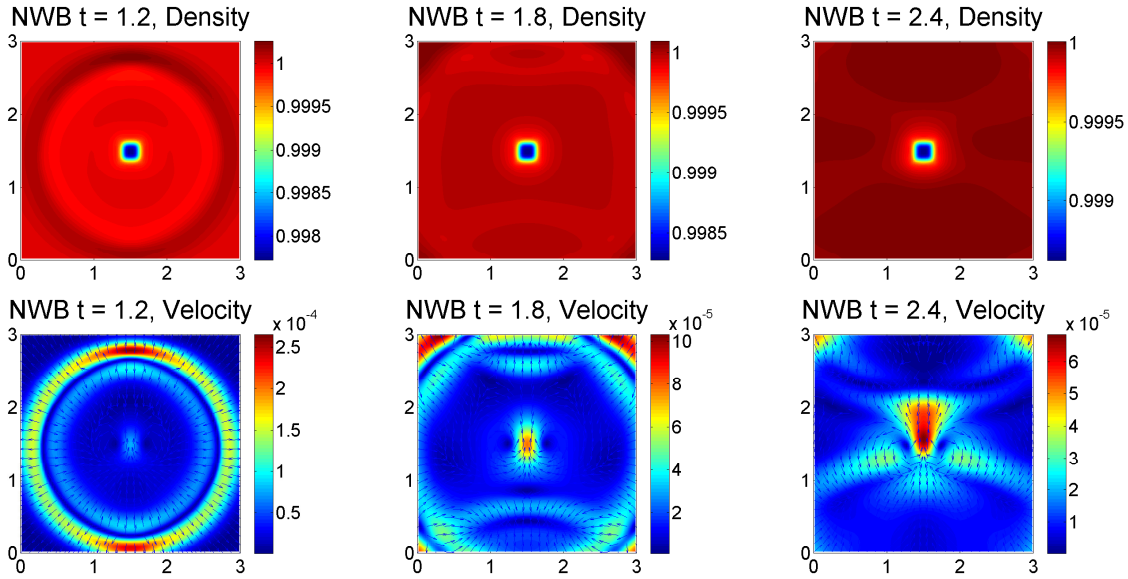

Figure 4.6: Example 4: Density (ρ) and velocity ($\sqrt{u^2+v^2}$) computed by the non-well-balanced CU scheme.

[2] A. Bollermann, G. Chen, A. Kurganov, and S. Noelle, *A well-balanced reconstruction of wet/dry fronts for the shallow water equations*, Journal of Scientific Computing, 56 (2013), pp. 267–290.

[3] N. Botta, R. Klein, S. Langenberg, and S. Lützenkirchen, *Well-balanced finite volume methods for nearly hydrostatic flows*, J. Comput. Phys., 196 (2004), pp. 539–565.

[4] S. Bryson, Y. Epshteyn, A. Kurganov, and G. Petrova, *Well-balanced positivity preserving central-upwind scheme on triangular grids for the Saint-Venant system*, M2AN

Math. Model. Numer. Anal., 45 (2011), pp. 423–446.

[5] A. Chertock, S. Cui, A. Kurganov, and T. Wu, *Well-balanced positivity preserving central-upwind scheme for the shallow water system with friction terms*, Internat. J. Numer. Meth. Fluids. Submitted.

[6] A. Chertock, M. Dudzinski, A. Kurganov, and M. Lukáčová-Medviďová, *Well-balanced schemes for the shallow water equations with coriolis forces*, (2014). Submitted.

[7] A. Chertock, A. Kurganov, and J. Miller, *Central-upwind scheme for a non-hydrostatic saint-venant system*. Submitted.

[8] U. S. Fjordholm, S. Mishra, and E. Tadmor, *Energy preserving and energy stable schemes for the shallow water equations*, in Foundations of computational mathematics, Hong Kong 2008, vol. 363 of London Math. Soc. Lecture Note Ser., Cambridge Univ. Press, Cambridge, 2009, pp. 93–139.

[9] ——, *Well-balanced and energy stable schemes for the shallow water equations with discontinuous topography*, J. Comput. Phys., 230 (2011), pp. 5587–5609.

[10] J. M. Gallardo, C. Parés, and M. Castro, *On a well-balanced high-order finite volume scheme for shallow water equations with topography and dry areas*, Journal of Computational Physics, 227 (2007), pp. 574–601.

[11] T. Gallouët, J.-M. Hérard, and N. Seguin, *Some approximate Godunov schemes to compute shallow water equations with topography*, Comput. & Fluids, 32 (2003), pp. 479–513.

[12] S. Gottlieb, D. I. Ketcheson, and C.-W. Shu, *Strong stability preserving Runge-Kutta and multistep time discretizations*, World Scientific Publishing Co. Pte. Ltd., Hackensack, NJ, 2011.

[13] S. Gottlieb, C.-W. Shu, and E. Tadmor, *Strong stability-preserving high-order time discretization methods*, SIAM Rev., 43 (2001), pp. 89–112.

[14] J. M. Greenberg and A. Y. Leroux, *A well-balanced scheme for the numerical processing of source terms in hyperbolic equations*, SIAM J. Numer. Anal., 33 (1996), pp. 1–16.

[15] S. Jin, *A steady-state capturing method for hyperbolic systems with geometrical source terms*, M2AN Math. Model. Numer. Anal., 35 (2001), pp. 631–645.

[16] R. Käppeli and S. Mishra, *Well-balanced schemes for the euler equations with gravitation*, Journal of Computational Physics, 259 (2014), pp. 199–219.

[17] A. Kurganov and D. Levy, *Central-upwind schemes for the saint-venant system*, M2AN Math. Model. Numer. Anal., 36 (2002), pp. 397–425.

[18] A. Kurganov and C.-T. Lin, *On the reduction of numerical dissipation in central-upwind schemes*, Commun. Comput. Phys., 2 (2007), pp. 141–163.

[19] A. KURGANOV, S. NOELLE, AND G. PETROVA, *Semi-discrete central-upwind scheme for hyperbolic conservation laws and Hamilton-Jacobi equations*, SIAM J. Sci. Comput., 23 (2001), pp. 707–740.

[20] A. KURGANOV AND G. PETROVA, *A second-order well-balanced positivity preserving central-upwind scheme for the saint-venant system*, Commun. Math. Sci., 5 (2007), pp. 133–160.

[21] A. KURGANOV AND E. TADMOR, *New high resolution central schemes for nonlinear conservation laws and convection-diffusion equations*, J. Comput. Phys., 160 (2000), pp. 241–282.

[22] ——, *Solution of two-dimensional riemann problems for gas dynamics without riemann problem solvers*, Numer. Methods Partial Differential Equations, 18 (2002), pp. 584–608.

[23] R. LEVEQUE, *Balancing source terms and flux gradients in high-resolution Godunov methods: the quasi-steady wave-propagation algorithm*, J. Comput. Phys., 146 (1998), pp. 346–365.

[24] R. LEVEQUE AND D. BALE, *Wave propagation methods for conservation laws with source terms*, in Proceedings of the 7th International Conference on Hyperbolic Problems, 1998, pp. 609–618.

[25] K.-A. LIE AND S. NOELLE, *On the artificial compression method for second-order nonoscillatory central difference schemes for systems of conservation laws*, SIAM J. Sci. Comput., 24 (2003), pp. 1157–1174.

[26] J. LUO, K. XU, AND N. LIU, *A well-balanced symplecticity-preserving gas-kinetic scheme for hydrodynamic equations under gravitational field*, SIAM J. Sci. Comput., 33 (2011), pp. 2356–2381.

[27] H. NESSYAHU AND E. TADMOR, *Nonoscillatory central differencing for hyperbolic conservation laws*, J. Comput. Phys., 87 (1990), pp. 408–463.

[28] S. NOELLE, N. PANKRATZ, G. PUPPO, AND J. NATVIG, *Well-balanced finite volume schemes of arbitrary order of accuracy for shallow water flows*, J. Comput. Phys., 213 (2006), pp. 474–499.

[29] S. NOELLE, Y. XING, AND C.-W. SHU, *High-order well-balanced schemes*, in Numerical methods for balance laws, vol. 24 of Quad. Mat., Dept. Math., Seconda Univ. Napoli, Caserta, 2009, pp. 1–66.

[30] B. PERTHAME AND C. SIMEONI, *A kinetic scheme for the Saint-Venant system with a source term*, Calcolo, 38 (2001), pp. 201–231.

[31] M. RICCHIUTO AND A. BOLLERMANN, *Stabilized residual distribution for shallow water simulations*, Journal of Computational Physics, 228 (2009), pp. 1071–1115.

[32] C.-W. SHU AND S. OSHER, *Efficient implementation of essentially non-oscillatory shock-capturing schemes*, J. Comput. Phys., 77 (1988), pp. 439–471.

[33] P. Sweby, *High resolution schemes using flux limiters for hyperbolic conservation laws*, SIAM J. Numer. Anal., 21 (1984), pp. 995–1011.

[34] C. T. Tian, K. Xu, K. L. Chan, and L. C. Deng, *A three-dimensional multidimensional gas-kinetic scheme for the navier-stokes equations under gravitational fields*, J. Comput. Phys., 226 (2007), pp. 2003–2027.

[35] B. van Leer, *Towards the ultimate conservative difference scheme. V. A second-order sequel to Godunov's method*, J. Comput. Phys., 32 (1979), pp. 101–136.

[36] Y. Xing and C.-W. Shu, *High order well-balanced WENO scheme for the gas dynamics equations under gravitational fields*, J. Sci. Comput., 54 (2013), pp. 645–662.

[37] Y. Xing, C.-W. Shu, and S. Noelle, *On the advantage of well-balanced schemes for moving-water equilibria of the shallow water equations*, J. Sci. Comput., 48 (2011), pp. 339–349.

[38] K. Xu, J. Luo, and S. Chen, *A well-balanced kinetic scheme for gas dynamic equations under gravitational field*, Adv. Appl. Math. Mech., 2 (2010), pp. 200–210.